scientific reports

Check for updates

OPEN

Leveraging explainable artificial intelligence with ensemble of deep learning model for dementia prediction to enhance clinical decision support systems

Mohamed Medani[1], Ghada Moh. Samir Elhessewi[2], Mohammed Alqahtani[3], Somia A. Asklany[4]✉, Sulaiman Alamro[5], Da'ad Albalawneh[6], Menwa Alshammeri[7] & Mohammed Assiri[8]

The prevalence of dementia is growing worldwide due to the fast ageing of the population. Dementia is an intricate illness that is frequently produced by a mixture of genetic and environmental risk factors. There is no treatment for dementia yet; therefore, the early detection and identification of persons at greater risk of emerging dementia becomes crucial, as this might deliver an opportunity to adopt lifestyle variations to decrease the risk of dementia. Many dementia risk prediction techniques to recognize individuals at high risk have progressed in the past few years. Accepting a structure uniting explainability in artificial intelligence (XAI) with intricate systems will enable us to classify analysts of dementia incidence and then verify their occurrence in the survey as recognized or suspected risk factors. Deep learning (DL) and machine learning (ML) are current techniques for detecting and classifying dementia and making decisions without human participation. This study introduces a Leveraging Explainability Artificial Intelligence and Optimization Algorithm for Accurate Dementia Prediction and Classification Model (LXAIOA-ADPCM) technique in medical diagnosis. The main intention of the LXAIOA-ADPCM technique is to progress a novel algorithm for dementia prediction using advanced techniques. Initially, data normalization is performed by utilizing min–max normalization to convert input data into a beneficial format. Furthermore, the feature selection process is performed by implementing the naked mole-rat algorithm (NMRA) model. For the classification process, the proposed LXAIOA-ADPCM model implements ensemble classifiers such as the bidirectional long short-term memory (BiLSTM), sparse autoencoder (SAE), and temporal convolutional network (TCN) techniques. Finally, the hyperparameter selection of ensemble models is accomplished by utilizing the gazelle optimization algorithm (GOA) technique. Finally, the Grad-CAM is employed as an XAI technique to enhance transparency by providing human-understandable insights into their decision-making processes. A broad array of experiments using the LXAIOA-ADPCM technique is performed under the Dementia Prediction dataset. The simulation validation of the LXAIOA-ADPCM technique portrayed a superior accuracy output of 95.71% over existing models.

Keywords Explainability artificial intelligence, Dementia prediction, Gazelle optimization algorithm, Data normalization, Feature selection

[1]Department of Information Systems, Applied College at Mahayil, King Khalid University, Abha, Kingdom of Saudi Arabia. [2]Department of Health Sciences, College of Health and Rehabilitation Sciences, Princess Nourah bint Abdulrahman University, P.O. Box 84428, 11671 Riyadh, Kingdom of Saudi Arabia. [3]Department of Information System and Cyber Security, College of Computing and Information Technology, University of Bisha, 61922 Bisha, Kingdom of Saudi Arabia. [4]Department of Computer Science and Information Technology, Faculty of Sciences and Arts, Northern Border University, 91431 Turaif, Arar, Kingdom of Saudi Arabia. [5]Department of Computer Science College of Computer, Qassim University, 51452 Buraydah, Kingdom of Saudi Arabia. [6]Department of Computer Science, University College in Umluj, University of Tabuk, Tabuk, Kingdom of Saudi Arabia. [7]Department of Computer Science, College of Computer and Information Sciences, Jouf University, Sakakah, Kingdom of Saudi Arabia. [8]Department of Computer Science, College of Computer Engineering and Sciences, Prince Sattam Bin

Abdulaziz University, P.O. BOX 16273, 3963 Al-Kharj, Kingdom of Saudi Arabia. ✉email: somia.asklany@nbu.edu.sa

Dementia is an advanced and irretrievable intellectual deterioration. There are forty million individuals suffer from dementia worldwide, and it is identified as a significant medical distress[1]. The dual main reasons for dementia are Alzheimer's disease (AD) and dementia initiated by vascular issues. It is responsible for seventy to eighty percent of cases distressing fifty million individuals[2]. Dementia symptoms are connected to ageing; nevertheless, few symptoms form at an initial stage. AD causes variations in the brain and affects the functional and structural features. Several neuropsychological and biological experiments find out AD might be forecast at its initial phase and beneficial to take therapy in an effective direction[3]. The growth of AD might have been predicted a few years before, which would have helped control the development of AD[4]. Positron emission tomography (PET), cerebrospinal fluid, Biomarkers, genetic data, and magnetic resonance imaging (MRI) are interested in detecting the initial symptoms of AD dementia. MRI offers multimode data for the brain's function and structure. MRI performs effectively to differentiate healthy individuals from survivors of AD[5]. For identifying dementia at an initial phase, the forecast model is vital to treat the disease. Dementia prevention approaches can vary in risks and costs. Samples of lower-risk and cost approaches would raise clinical attention and counselling on living[6]. Risks and costs rise if specified drugs are deliberated, changing risky aspects and directly affecting the disease process. A variety of people for lower cost and risk interferences should take individuals with the probable disease, even at the cost of sampling subjects, who will not get the illness. In this instance, the forecast is sensitive, even if positive predictive value (PPV) and higher specificity cannot be accomplished[7]. If there is interference of higher risk or cost, choice is limited to those who will probably progress the illness at the possible cost of missing a few. A device that gives a constant score instead of a fixed categorical definition to give diverse stages of sensitivity, PPV, and specificity by utilizing various cut-offs[8]. AD forecasts utilizing ML methods are stated in diverse medical experiments[9]. A detailed study centres on supervised learning methods for solving concerns in different fields and supervised learning approaches for recognizing multiple illnesses using multiple computer-assisted methods. ML is deliberated as an essential part of artificial intelligence (AI) and a data analysis model that automates the explanatory technique framework[10]. ML models are gradually employed in neuroimaging analysis, such as an AD prediction from auxiliary MRI. Therefore, computer-assisted ML methods have been implemented for integrative examinations.

This study introduces a Leveraging Explainability Artificial Intelligence and Optimization Algorithm for Accurate Dementia Prediction and Classification Model (LXAIOA-ADPCM) technique in medical diagnosis. The main intention of the LXAIOA-ADPCM technique is to progress a novel algorithm for dementia prediction using advanced techniques. Initially, data normalization is performed by utilizing min–max normalization to convert input data into a beneficial format. Furthermore, the feature selection process is performed by implementing the naked mole-rat algorithm (NMRA) model. For the classification process, the proposed LXAIOA-ADPCM model implements ensemble classifiers such as the bidirectional long short-term memory (BiLSTM), sparse autoencoder (SAE), and temporal convolutional network (TCN) techniques. Finally, the hyperparameter selection of ensemble models is accomplished by utilizing the gazelle optimization algorithm (GOA) technique. Finally, the Grad-CAM is employed as an XAI technique to enhance transparency by providing human-understandable insights into their decision-making processes. A broad array of experiments using the LXAIOA-ADPCM technique is performed under the Dementia Prediction dataset.

- The LXAIOA-ADPCM model utilizes min–max normalization to standardize the data, ensuring consistent input ranges. This technique improves the technique's capability to process and learn from the data effectually. Enhancing data consistency contributes to more accurate and reliable model performance.
- The LXAIOA-ADPCM method employs the NMRA technique for feature selection, which detects the most relevant features for classification. This methodology mitigates dimensionality and enhances model efficiency. Concentrating on the most informative features and mitigating noise and irrelevant data improves the model's accuracy.
- The LXAIOA-ADPCM approach employs a combination of ensemble classifiers, such as BiLSTM, SAE, and TCN, to leverage their complementary merits. This approach improves the model's capability to capture intrinsic patterns in the data. By incorporating these techniques, the model attains higher accuracy and robustness in classification tasks.
- The LXAIOA-ADPCM methodology implements the GOA model for hyperparameter selection, fine-tuning the model for optimal performance. This method effectively searches for the optimal hyperparameters, enhancing the model's accuracy and generalization. Optimizing key parameters ensures improved model efficiency and robust results across diverse tasks.
- Grad-CAM is an XAI technique that visualizes and interprets the model's decision-making process. It underscores crucial features and regions in the data, enhancing the model's transparency. This enables users to understand how the model arrives at its predictions, improving trust and interpretability.
- The LXAIOA-ADPCM model introduces a unique integration of the NMRA, ensemble classifiers, GOA for hyperparameter selection, and Grad-CAM for improved explainability. This integration enhances the accuracy and interpretability of complex classification tasks. The novelty is seamlessly blending optimization, classification, and explainability techniques to address real-world threats effectively.

Review of Literature

In[11], an innovative interpretable method is projected to integrate EBM and CNN for identification and AD prediction. This work progresses a novel training model that alternately trains the CNN module as a feature extractor and the EBM element as the output block to develop an end-to-end technique. This method acquires

imaging data as input and offers predictions or interpretable feature significant processes. In[12], a hybrid CNN-LSTM-based method is projected for forecasting AD development depending on the fusion of 4 longitudinal reasoning subscores procedures. This hybrid method utilizes the Bayesian optimizer as a computational model to enhance the choice of sufficient DL structure. A genetic algorithm (GA)-based FS is integrated as a level of optimization to establish the finest feature set from the removed CNN-LSTM deep representations, and the conventional SoftMax (SM) classifier is substituted for an optimized and strong random forest (RF) classifier. Arshad Choudhry et al.[13] developed an innovative model for explainability in graph convolutional neural networks (GCNN). Using conventional CNN interpretability devices like CAM, EB, and saliency maps frequently does not manage the intricacy of graph-structured data. This method also projects dual innovative devices: contrastive EB for deeper insights into functions and adaptive CAM for differentiated interpretability. Utilizing an innovative feature fusion method, this technique further pushes the limitations and incorporates the feature assets of CNN and GNN for a holistic knowledge of GCNN decision-making. AbdelAziz et al.[14] projected the Squeeze-and-Excitation CNN with RF (SECNN-RF) structure for timely AD recognition utilizing MRI scans. The SECNN-RF combines Squeeze-and-Excitation (SE) blocks into CNN aimed at essential aspects and utilizes Dropout layers to preclude over-fitting. It utilizes an RF classifier to classify the removed aspects precisely. Bazine et al.[15] developed an innovative deep few-shot learning model for MRI-based AD identification. This technique contains dual encoders and a single decoder, receives dual image modalities like cross-section and longitudinal MRI, and creates a novel cross-section image. A skip connection approach is also determined among the primary encoder and decoder, like the UNet mechanism. Kamal and Nimmy[16] developed a novel method by employing a multimodal data-specific model that implements converters to either image or textual data. During the primary phase, data pre-processing for multimodal databases is addressed using a U-net-based segmentation model, effectually isolating the Region of Interest (ROI) in MRI images. Another phase involves the employment of BERT and vision transformers (ViT) to process the pre-processed data. Khanom et al.[17] projected an ensemble boosting machine, PD-EBM, to recognize PD. PD-EBM utilizes ML models and a hybrid FS method to improve analytical precision. Whereas ML has revealed promise in clinical applications to recognize PD, the intelligibility of these methods endures a major problem. Explainable ML (XML) addresses this by providing clarity and transparency when predicting models.

Adarsh et al.[18] developed a novel analytical structure that synergizes CNN with MKSCDDL. This integrative model is intended to assist in accurately classifying individuals into classifies of mild cognitive impairment (MCI), cognitively normal (CN), and AD ranks while discriminating the nuanced stages in the MCI spectrum. This method is identified by its interpretability and robustness, providing a therapist with exceptionally transparent devices for identifying and formulating therapeutic approaches. Alhussen et al.[19] propose an advanced attention-deficit/hyperactivity disorder (ADHD) detection framework that incorporates NeuroDCT-ICA for EEG pre-processing, RhinoFish Optimization for feature selection, and ADHD-AttentionNet for accurate and stable ADHD detection. Zhang et al.[20] analyze the safety and efficacy of hematoma evacuation utilizing an image-guided para-corticospinal tract approach, concentrating on protecting the corticospinal tract during surgery. Pei et al.[21] explore the potential of quercetin-functionalized nanomaterials to improve quercetin's delivery and therapeutic effects in AD by enhancing solubility, stability, and blood–brain barrier penetration. Pan et al.[22] present a novel EEG-based image reconstruction methodology by utilizing a deep visual representation model (DVRM) model to improve the quality of reconstructed visual stimuli images. Pan et al.[23] propose a decision-level fusion scheme for mental state evaluation utilizing multidomain EEG information, optimized through support vector machine (SVM), k-nearest neighbour (kNN), and backpropagation (BP) networks, and to detect the best fusion algorithm for accurate assessment in a coal mine environment. Wang et al.[24] explore strategies for enhancing the surgical management of intracerebral haemorrhage (ICH) by reducing iatrogenic harm to the corticospinal tract and improving neurological prognosis through endoscopic hematoma evacuation. Li et al.[25] develop a sensitive and specific miRNA detection approach for myocarditis utilizing tyramine signal amplification integrated with enzyme catalysis, enabling the detection of acute myocarditis patients through colourimetric analysis. Chauhan et al.[26] propose the Patch Base ViT (PBVit) technique for brain tumour detection, improving diagnostic accuracy by employing a patch-based approach for enhanced pattern recognition in brain scans. Walha et al.[27] develop a speech-based dementia detection model utilizing Parallel Recurrent Convolutional Neural Networks (PRCNN), Average stochastic gradient descent Weight-Dropped Long Short-Term Memory (AWD-LSTM), and Densenet, attaining high accuracy and low computational complexity. Freja and Hallaj[28] aim to detect dementia by analyzing speech patterns using ML and large language models (LLMs) models.

The limitations of the existing studies comprise the reliance on specific datasets (e.g., Pitt Corpus) that may not fully represent diverse populations, potentially restricting generalizability. Furthermore, many models, such as CNN, LSTM, and RF, are computationally intensive, which may affect real-time application in clinical settings. There is also a lack of multimodal data integration, which could improve the model's performance. Moreover, interpretability remains a challenge, specifically in complex models like GNNs and deep fusion techniques. Lastly, applying the models in clinical practice is still limited, as many are in the early stages of development and require additional validation. The absence of standardized benchmarks for cross-domain comparisons and limited integration of patient-specific factors restrict progress toward more personalized and effective healthcare solutions.

The proposed methodology

This paper proposes an LXAIOA-ADPCM method for medical diagnosis. The main intention of the LXAIOA-ADPCM method is to progress a novel technique for dementia prediction using advanced techniques. It contains various processes involved, such as min–max normalization, NMRA-based feature selection, ensemble of dementia prediction model, parameter tuning, and XAI using Grad-CAM. Figure 1 represents the entire procedure of the LXAIOA-ADPCM model.

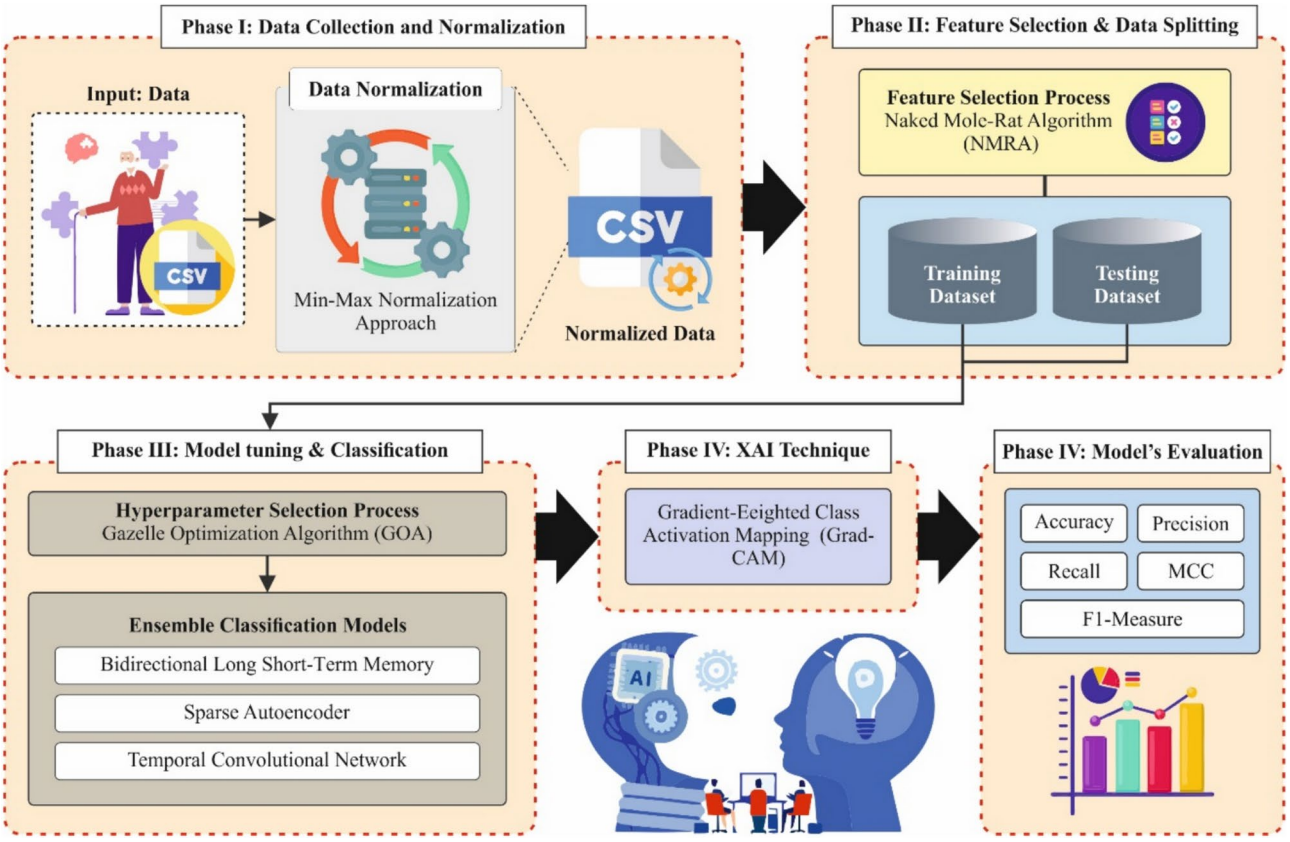

Fig. 1. Overall process of LXAIOA-ADPCM approach.

Min–max normalization

At first, the data normalization stage employs min–max normalization for converting input data into a beneficial format[29]. This is chosen for its simplicity and efficiency in transforming data into a consistent scale, typically between 0 and 1. This technique assists in preventing the model from being biased towards features with more extensive numerical ranges, ensuring fair treatment of all features. Compared to other normalization methods, namely Z-score standardization, Min–Max normalization is proper when the model requires the data to be within a specific range, improving the performance of algorithms sensitive to feature scale. It also confirms that features with varying scales don't dominate the learning process, resulting in more accurate predictions and enhanced model stability. Furthermore, it is computationally efficient, making it appropriate for massive datasets and real-time applications.

Min–max normalization is a data pre-processing method employed to measure features in a fixed range, usually [0, 1] or [−1, 1]. In the prediction of dementia, it certifies that every input variable donates similarly to the method, averting dominance by features with greater numerical values. This method enhances the convergence speed, model stability, and accuracy by upholding the relative relations among data points. Min–max normalization is chiefly beneficial when allocating medical datasets with fluctuating scales and units. It maintains the distribution of original data while improving the performance of the ML model. Converting features into an even range simplifies better pattern detection and classification in the diagnosis of dementia.

NMRA-based feature selection

Besides, the FS process is performed by implementing the NMRA model[30]. This method is chosen due to its robust exploration and exploitation capabilities, which are significant for detecting the most relevant features in high-dimensional data. Unlike conventional methods, NMRA replicates the adaptive strategies of the naked mole-rat to efficiently search the solution space, averting local optima and ensuring a more comprehensive exploration of potential feature subsets. This is advantageous for complex datasets where conventional feature selection methods, like Recursive Feature Elimination (RFE) or GAs, may face difficulty with large or noisy data. By utilizing NMRA, the model can attain optimal feature subsets that improve classification accuracy and mitigate computational complexity. Additionally, its capability to balance exploration and exploitation makes it highly effective in dynamic and uncertain environments, confirming robust feature selection even in the presence of irrelevant or redundant features. This model mimics the natural mating behaviours of Naked mole rats. This approach is separated into 3 phases. The initial phase is designated as the initialization phase, the worker phase is the second phase, and the breeder phase is the last.

Initialization

This phase is most often found in bio-inspired methods. Typically, it is the last phase of the bio-inspired model. During NMRA, the early range of the population is $[1, 2, 3, 4, 5, 6, \ldots, n]$, and the vector of the dimension (D). The mathematical representation is provided in Eq. (1).

$$K_{ij} = K_{\min j} + R(0,1) * (K_{\min j} - K_{\max j}) \tag{1}$$

Meanwhile, the variables $K_{\min j}$ and $K_{\max j}$ characterize the lower and upper limits of the specified function correspondingly. The variable i was described in the interval of 1 to n, while the variable j is described in the interval of 1 to D. Following the initialization stage, the objective function fitness is assessed, and workers (W) and breeders (B) are established.

Worker

After executing the initialization phase, a resolution of the objective function fitness. This assessment exemplifies a basis for determining the workers (W) and breeders (B). During this phase, the workers improve their fitness, such as their probability of becoming a breeder and m, dating w, with the queen. Accordingly, the worker Naked Mole-Rat creates novel solutions based on knowledge. When the novel solution is the finest, the novel optimal solution is substituted by the older one. Or else utilize the older optimal solution. Finally, the mathematical representation of the optimal solution is represented by Eq. (2).

$$Z_i^{t+1} = Z_i^t + \lambda \left(Z_j^t - Z_k^t\right) \tag{2}$$

whereas novel solution $\left(Z_i^{t+1}\right)$, preceding solution $\left(Z_i^t\right)$, mating feature ($\lambda = [0, 1]$), and arbitrarily selected solution $\left(Z_j^t - Z_k^t\right)$ from the worker pool.

Breeder

Besides being chosen to mate in addition to continued breeders, the breeder, Naked Mole-Rat, might preserve himself upgraded. Nevertheless, some breeders cannot enhance their fitness, and they might return to worker pooling. Hence, Eq. (3) offers the mathematical representation for novel breeder solutions.

$$P_i^{t+1} = (1 - \lambda) P_i^t + \lambda \left(d - P_i^t\right) \tag{3}$$

whereas the λ parameter (while $\lambda = (0, 1)$ influences the breeding frequency between the queen and the breeder. The novel solution at time $t + 1$ is represented as P_i^{t+1}, the complete optimal solution is characterized by d, and the solution of the breeder at t he time is signified as P_i^t.

The fitness function (FF) imitates the classifier's accuracy and the quantity of chosen features. It exploits classification accuracy and diminishes the set dimension of preferred features. Therefore, the FF below is applied to assess individual solutions, as in Eq. (4).

$$Fitness = \alpha * ErrorRate + (1 - \alpha) * \frac{\#SF}{\#All\_F} \tag{4}$$

Here, $ErrorRate$ denotes the classifier rate of error utilizing the chosen feature. $ErrorRate$ is intended as the proportion of incorrect categories to the number of classifications made between 0 and 1. $\#SF$ denotes the number of nominated features, and $\#All\_F$ refers to the complete number of features in the dataset. α is employed to influence the impact of classifier quality and length of the subset.

Ensemble of dementia prediction model

The proposed LXAIOA-ADPCM model utilizes ensemble classifiers such as the BiLSTM, SAE, and TCN techniques for classification. This ensemble classifier employs the merits of each method to improve classification performance. BiLSTM captures past and future contextual data through its bidirectional architecture, making it highly effective for sequential data analysis. SAE helps with dimensionality reduction and feature learning by efficiently compressing input data while maintaining key information. TCN, with its convolutional layers, outperforms modelling long-range dependencies and temporal patterns. Integrating these models in an ensemble approach allows the system to benefit from their complementary strengths, resulting in more robust and accurate classification. This hybrid strategy assists the model in adapting to various data types and attack scenarios, ensuring improved generalization and resilience compared to individual classifiers alone.

BiLSTM classifier

BiLSTM is based on bidirectional RNN (Bi-RNN) that utilizes dual different hidden layers (HLs) for processing the input sequences from forward and reverse orientations[31]. Bi-LSTMs join either HL to an individual output layer. Conventional RNNs are restricted because they can only use the preceding context of the input data stream. BiLSTM corrects this problem by allocating information in forward and backward orientations. Figure 2 depicts the structure of BiLSTM.

The Bi-LSTM theory derives from Bi-RNN handling the data sequence in either forward or reverse directions and utilizing dual different HLs. It associates dual HLs to the single output layer. One insufficiency of conventional RNNs is that they are only adequate for using the preceding context. Bi-RNNs resolve this by distributing data

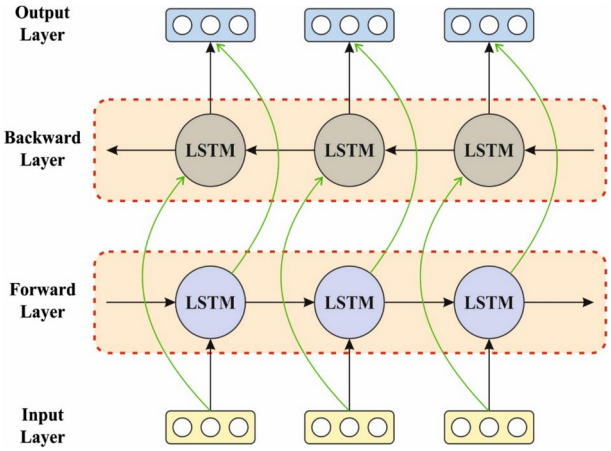

Fig. 2. Architecture of BiLSTM.

in either direction. The Bi-RNN computes the output sequence y, the backward hidden sequence $\overline{n}$, and the forward hidden sequence $\overline{n}$ by iterating the layer of backward from $t = T$ to 1, the layer of forward from $t = 1$ to T and then upgrading the output layer by the succeeding equations:

$$\vec{\mathrm{h}} = \mathcal{H}\left(W_{x\vec{\mathrm{h}}}x_t + W_{\vec{\mathrm{h}}\vec{\mathrm{h}}}\vec{\mathrm{h}}_{t+1} + b_{\vec{\mathrm{h}}}\right) \tag{5}$$

$$\overleftarrow{\mathrm{h}} = \mathcal{H}\left(W_{x\overleftarrow{\mathrm{h}}}x_t + W_{\overleftarrow{h}\,\overleftarrow{h}}\overleftarrow{\mathrm{h}}_{t+1} + b_{\overleftarrow{\mathrm{h}}}\right) \tag{6}$$

$$y_t = W_{\vec{\mathrm{h}}y}\vec{\mathrm{h}}_t + W_{\overleftarrow{\mathrm{h}}\,y}\overleftarrow{\mathrm{h}}_t + b_y \tag{7}$$

The Bi-LSTM layer provides a vector of output, YT, that is calculated by the equation:

$$y_t = \sigma\left(\vec{\mathrm{h}}_t.\overleftarrow{\mathrm{h}}_t\right) \tag{8}$$

whereas σ function associations either the sequence of output. The σ function has four types: average concatenating, multiplication function, and summation.

SAE method

It considers a single d-dimensional feature vector an individual SAE training sample, excluding information over this spatial location[32]. Then, how are training samples obtained from every feature mapping? The time step index t in the following representations is dropped for simplification.

Let $x \in \mathbb{R}^d$ signify the d-dimensional activation vectors from an individual location of a feature mapping and let n remain latent size in SAE. The decoder and encoder of normal single-layer $ReLU$ SAE are then described as demonstrated:

$$\begin{aligned} z &= ReLU\left(W_{enc}\left(x - b_{pre}\right) + b_{enc}\right) \\ \hat{X} &= W_{dec}z + b_{pre} \end{aligned} \tag{9}$$

whereas $W_{enc} \in \mathbb{R}^{n\times d}$ and $W_{dec} \in \mathbb{R}^{d\times n}$ are encoders and decoder weighting matrices individually, $b_{pre} \in \mathbb{R}^d$ and $b_{enc} \in \mathbb{R}^n$ are learnable biased terms. Components of z-named activations of the feature are typically represented as $f_{1,\ldots,n}(x)$. Usually, n is equivalent to d multiplied by a positive expansion factor.

The SAE objective function is described as:

$$\mathcal{L}(x) = \left\|x - \hat{X}\right\|_2^2 + \alpha\mathcal{L}_{aux} \tag{10}$$

whereas $\left\|x - \hat{X}\right\|_2^2$ denotes error of reconstruction, $\mathcal{L}_{aux}$ signifies error of reconstruction utilizing only the leading $_{faux}$ activations of the feature, which have not been experienced on a more significant number of training instances, referred to as dead latent. The loss of auxiliary has been applied to avoid dead latent and is scaled by the coefficient α.

TCN model

TCN uses neural networks to analyze time series data[33]. It applies components like residual block (RB), dilated convolution (DC), and causal convolution (CC) to remove longer-term temporal designs. Complete descriptions of all components are in the succeeding sub-sections.

CCs are an essential portion of the TCN structure, permitting the system to produce outputs the same length as their inputs without integrating upcoming data. For time-series input $X = (x_0, x_1, \ldots, x_t)$, the output y_t at tth time is only depending on inputs at the current time and limited previous times $(x_t, x_{t-1}, x_{t-2}, x_{t-3})$ whereas no upcoming inputs are applied $(x_{t+1}, x_{t+2}, \ldots, x_{t+T})$. X characterizes the input sequence of time series data, while all components x_i are associated with the time step within the sequence. The output y_t at all times t only relies on inputs up to x_t, guaranteeing that no upcoming data is combined.

CC carefully preserves the sequential order of the outputs and inputs such that the output at time t relies only on an input up to time $t-1$ within the prior layer. This architecture allows the method to progressively grow knowledge of the sequence of inputs while preventing the presence of upcoming data in present predictions. This succeeds mostly for time-sensitive uses, namely STLF.

To overcome the issue of narrow field accessibility related to CCs, TCN presents DCs. DCs expand the receptive area by permitting the convolution input to cover various intervals. Improving the dilation featured, in addition to the filter k's dimension, permits taking long-term dependences in the input time series. Therefore, the topmost layers can agree with various input data in this model selection.

$$H_T(X, f) = \sum_{i=0}^{k-1} f(i) \cdot x_{T-di} \tag{11}$$

whereas $X = (x_0, x_1, \ldots, x_t, \ldots, x_T)$ characterizes 1D time series input, $H_T(\cdot)$ signifies the DC process on the sequence component T, f, and d specifies the filter and dilation feature, k refers to the dimension of the filter, and $T - di$ specifies the previous direction. Modifying the receptive field develops, permitting the method to seizure dependences through a higher range of data. This extended receptive area is essential for tasks, whereas understanding long-range dependencies can improve the prognostic precision of the method.

RBs are applied in TCN to successfully overwhelm the challenges related to training intense networks and alleviate the vanishing gradient problems. The RB contains dual branches. The initial utilizes a transformation process named $F(\cdot)$ on input X_{h-1}. The next one implements a 1x1 convolution process to preserve the number of feature maps stable. The output X_h of the hth RB is as shown:

$$X_h = \delta(F(X_{h-1}) + X_{h-1}) \tag{12}$$

whereas $\delta(\cdot)$ denotes activation procedure, generally $ReLU$ which presents non-linearity to assist the system learning composite models, and $F(\cdot)$ epitomizes a transformation series employed to X_{h-1}, the input to these blocks, and contains processes such as CC, DC, WeightedNorm normalization, and dropout typically. The stacked RBs in TCN permit the system to remove features through an extensive input temporal range.

Parameter tuning using GOA

Eventually, the hyperparameter selection of ensemble models is performed by employing the GOA method[34]. This technique is chosen because it can effectively explore complex search spaces and optimize hyperparameters. GOA replicates the natural behaviour of gazelles, enabling it to escape local optima and effectively balance exploration and exploitation. This is significant in hyperparameter optimization, where finding the optimal parameters can significantly improve the model's performance. Compared to other optimization techniques, such as grid or random search, GOA is more adaptive and efficient, needing fewer iterations to converge to an optimal solution. Its flexibility makes it ideal for tuning parameters in DL methods, ensuring improved accuracy and mitigated overfitting. Additionally, the strong convergence properties of the GOA method allow it to perform well across diverse datasets and task complexities.

The GOA is stimulated by the gazelle's survival behaviours in their natural environment. This method mimics these behaviours to solve optimizer issues effectively by balancing exploitation and exploration in the searching region.

Initialization of the population

The GOA serves as the population-based method, using the collection of gazelles, or search agents, which are primarily distributed arbitrarily through the searching region. These agents are designed into the matrix P of dimension $m \times n$, while m denotes gazelle counts and n embodies the optimizer problem dimensionality. All matrix elements are associated with possible solutions by their values limited by the problem's lower (L) and upper (U) limits. The initialization of the locations is specified by:

$$P = \begin{pmatrix} p_{1,1} & p_{1,2} & \cdots & p_{1,n-1} & p_{1,n} \\ p_{2,1} & p_{2,2} & \cdots & p_{2,n-1} & p_{2,n} \\ \vdots & \vdots & \ddots & \vdots & \vdots \\ p_{m,1} & p_{m,2} & \cdots & p_{m,n-1} & p_{m,n} \end{pmatrix} \tag{13}$$

Now, $p_{i,j}$ signifies the location of the ith gazelle in the jth size, calculated utilizing:

$$p_{i,j} = rand \times (U_j - L_j) + L_j \tag{14}$$

On the other hand, $rand$ denotes a randomly generated number amongst (0, 1). This equation guarantees that the first locations are distributed within the described limits.

As the model advances, all positions of the gazelle are assessed, making candidate solutions. The optimal solution originating at some point is selected as the best gazelle, and its location is applied to make the elite matrix, managing the search procedure in the following iterations. The elite matrix is upgraded after all iterations if a better solution is discovered, as presented in:

$$E = \begin{pmatrix} e_{1,1} & e_{1,2} & \cdots & e_{1,n-1} & e_{1,n} \\ e_{2,1} & e_{2,2} & \cdots & e_{2,n-1} & e_{2,n} \\ \vdots & \vdots & \ddots & \vdots & \vdots \\ e_{m,1} & e_{m,2} & \cdots & e_{m,n-1} & e_{m,n} \end{pmatrix} \tag{15}$$

In this matrix, $e_{i,j}$ signifies the location of the best-performing gazelle, which is essential for refining the direction of the search.

Brownian motion (BM)

BM defines an arbitrary movement while the displacement emulates Gaussian distributions, considered by the variance σ 2 = 1 and mean μ = 0. The likelihood density function for BM at some location *y* is stated as:

$$f_B(y; \mu, \sigma) = \frac{1}{\sqrt{2\pi\sigma^2}} \exp\left(-\frac{(y-\mu)^2}{2\sigma^2}\right) \tag{16}$$

This function summarizes the randomness associated with BM.

Lévy flight (LF)

LF characterizes other types of random walk, considered by step lengths, which emulate a power-law distribution. This permits random longer jumps that improve exploration abilities.

$$L(z_j) \sim \frac{1}{z_j^{1+\beta}} \tag{17}$$

whereas z_j refers to step length, and β means exponent, commonly among (1, 2). The Lévy stable procedure, leading these behaviours, is defined by the integral:

$$f_L(z; \beta, \gamma) = \frac{1}{\pi} \int_0^\infty \exp\left(-\gamma q^\beta\right) \cos(qz)\, dq \tag{18}$$

Now, β impacts the characteristics distribution, whereas γ denotes the scaling parameter. The model utilizes a model to make LFs with β values range between 0.3 to 1.99, determined by:

$$Levy(\beta) = 0.05 \times \frac{z}{|w|^{\frac{1}{\beta}}} \tag{19}$$

whereas z and w are derived from standard distributions:

$$z = Normal\left(0, \sigma_z^2\right) \tag{20}$$

$$w = Normal\left(0, \sigma_w^2\right) \tag{21}$$

with:

$$\sigma_z = \left[\frac{\Gamma(1+\beta)\sin\left(\frac{\pi\beta}{2}\right)}{\Gamma\left(\frac{1+\beta}{2}\right)\beta 2^{\frac{\beta-1}{2}}}\right] \tag{22}$$

$$\sigma_w = 1 \tag{23}$$

$$\beta = 1.5 \tag{24}$$

These equations define the LF implementation inside the GOA, assisting in effectively exploring the searching region.

Exploitation stage

In the exploitation stage, the gazelles are regarded as grazing gently, for lack of a predator or after the predator quietly observes them. The movement of the gazelle in this stage is modelled utilizing BM and involves constant

and efficient stages for effectively exploring the area. The mathematic representation of this grazing behaviour is provided in Eq. (25):

$$g_{k+1} = g_k + v \cdot R \cdot B \cdot (E_k - B \cdot g_k) \tag{25}$$

Here, g_{k+1} characterizes the location of the gazelle at the following step, g_k denotes the present location, v symbolizes the grazing speed, B refers to the vector having arbitrary values to mimic BM, and R stands for the vector of random values distributed uniformly inside the range [0,1].

Exploration stage
This stage originates after the gazelles identify predators. Upon sensing danger, the gazelles show behaviours like foot-stomping, stotting (high leaps), or tail flicking that are represented mathematically by scaling a randomly generated value among (0, 1). The movement of the gazelle in this stage follows an LF design, considered by the mixture of shorter phases and random long jumps that improve the model's exploration abilities. Once the predator is identified, the gazelles start running directly, whereas the predator offers pursuit. The predator or the gazelles make quick directional changes in the search, characterized by the parameter α. This method implies these directional variations take place at all iterations by the gazelle moving in all directions in odd-numbered iterations and the opposed direction in even-numbered iterations. Primarily, the gazelle uses LF, whereas the predator begins with a BM design before transferring to LF. The mathematic representation for the movement of gazelles afterwards distinguishing the predator is presented in Eq. (26):

$$g_{k+1} = g_k + V \cdot \alpha \cdot L \cdot (E_k - L \cdot g_k) \tag{26}$$

Now, V means the maximal speed the gazelle can attain, and L refers to a vector of arbitrary values originating from the distributions of Lévy. The mathematic representation for the chasing behaviour of the predator is specified in Eq. (27):

$$g_{k+1} = g_k + V \cdot \alpha \cdot PF \cdot B\,(E_k - L \cdot g_k) \tag{27}$$

Now, PF signifies the cumulative effect of the predator, described as:

$$PF = 1 - \left(\frac{k}{MaxIter}\right)^{2\left(\frac{k}{MaxIter}\right)} \tag{28}$$

$$g_{k+1} = \begin{cases} g_k + PF \cdot [LB - R \cdot (UB - LB)] \cdot U & if r < PSR \\ g_k + [PSR\,(1-r) + r] \cdot (g_{r1} - g_{r2}) & otherwise \end{cases} \tag{29}$$

In this method, U denotes a binary vector made by a randomly generated number r inside the interval [0,1], whereas:

$$U = \begin{cases} 0 & if\ r < PSR \\ 1 & otherwise \end{cases} \tag{30}$$

The indices r_1 and r_2 are random selections from the gazelle matrix, demonstrating the gazelles' dissimilar locations in the population. The GOA originates an FF to amend the classifier's performance. It determines an optimistic number to signify the better efficiency of the candidate outcome. The classifier rate of error reduction is measured as FF, as assumed in Eq. (31).

$$\begin{aligned} &fitness\,(x_i) = Classifier\ Error\ Rate\,(x_i) \\ &= \frac{no.\ of\ misclassified\ samples}{Total\ no.\ of\ samples} \times 100 \end{aligned} \tag{31}$$

XAI using Grad-CAM

At last, Grad-CAM model is employed as an XAI technique to enhance transparency by providing human-understandable insights into their decision-making processes[35]. This model is chosen for its capability to provide visual explanations by emphasizing the regions of an input image that contribute most to the prediction of the model. It is specifically useful in CNN-based models, allowing for an intuitive understanding of how the model makes decisions. This technique improves model interpretability, giving insight into feature importance and improving trustworthiness in decision-making processes.

During DL, every CNN method contains classification and feature extraction branches. The classification branch controls a layer of FC, and the recovered information of DL has been converted into likelihood values for every label within the layer of SM. This last categorized result of the approach represents a label through the maximal probability values. Grad-CAM, the final XAI model utilized in these works, helps as a class-discriminating localization approach that can facilitate graphic understanding without requiring structural modifications or retraining. It accomplishes this by restricting related sampled areas and using the gradient data of the activation mapping DL from the last convolution layers to underline parts of the sample by the critical influence on the probability value for the forecast result. Areas with a greater gradient are symptomatic of the region using a considerable impact on the prediction consequences. The output of Grad-CAM is established

Group	No. of samples
Nondemented	190
Demented	146
Converted	37
Total samples	373

Table 1. Details of the dataset.

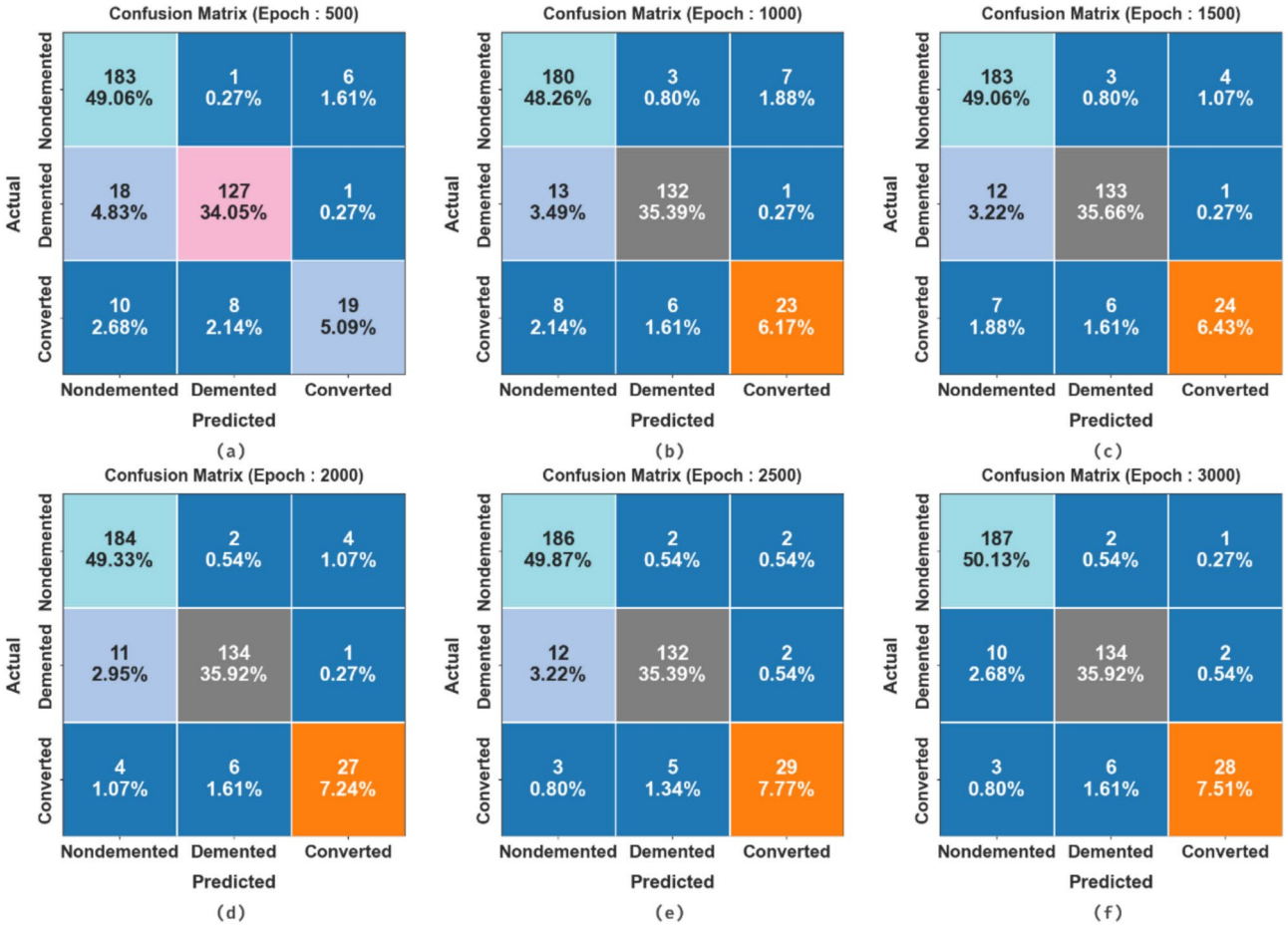

Fig. 3. Confusion matrix of LXAIOA-ADPCM methodology (**a**–**f**) epochs 500–3000.

as a heat map visualization equivalent to particular classes. This heat map is active in graphically checking the regions of interest inside the image, as described within the investigational study segment.

Experimental validation

Here, the performance analysis of the LXAIOA-ADPCM technique is inspected under the Dementia Prediction dataset[36]. This dataset contains 373 samples in three groups. Table 1 depicts the complete details of this dataset. The dataset contains 14 features, but only 10 features are selected.

Figure 3 represents the confusion matrices produced by the LXAIOA-ADPCM methodology under several epochs. The results recognize that the LXAIOA-ADPCM approach detects and identifies every class label specifically.

The classifier outcomes of the LXAIOA-ADPCM technique are determined below dissimilar epochs in Table 2 and Fig. 4. The outcomes state that the LXAIOA-ADPCM technique properly recognized all the samples. On epoch 500, the LXAIOA-ADPCM technique attains an average $accu_y$ of 92.14%, $prec_n$ of 84.40%, $reca_l$ of 78.22%, $F1_{Measure}$ of 80.55%, and MCC of 74.58%. Besides, on epoch 1000, the LXAIOA-ADPCM methodology achieves an average $accu_y$ of 93.21%, $prec_n$ of 85.79%, $reca_l$ of 82.44%, $F1_{Measure}$ of 83.90%, and MCC of 78.42%. Also, on epoch 1500, the LXAIOA-ADPCM methodology accomplishes an average $accu_y$ of 94.10%, $prec_n$ of 89.00%, $reca_l$ of 84.09%, $F1_{Measure}$ of 86.15%, and MCC of 81.52%. Moreover, on epoch 2000, the LXAIOA-ADPCM methodology gains an average $accu_y$ of 95.00%, $prec_n$ of 90.40%, $reca_l$ of 87.20%,

Class labels	$Accu_{racy}$	$Prec_{n}$	$Reca_{l}$	$F1_{measure}$	MCC
Epoch—500					
Nondemented	90.62	86.73	96.32	91.27	81.71
Demented	92.49	93.38	86.99	90.07	84.19
Converted	93.30	73.08	51.35	60.32	57.83
Average	92.14	84.40	78.22	80.55	74.58
Epoch—1000					
Nondemented	91.69	89.55	94.74	92.07	83.50
Demented	93.83	93.62	90.41	91.99	87.01
Converted	94.10	74.19	62.16	67.65	64.74
Average	93.21	85.79	82.44	83.90	78.42
Epoch—1500					
Nondemented	93.03	90.59	96.32	93.37	86.22
Demented	94.10	93.66	91.10	92.36	87.58
Converted	95.17	82.76	64.86	72.73	70.75
Average	94.10	89.00	84.09	86.15	81.52
Epoch—2000					
Nondemented	94.37	92.46	96.84	94.60	88.83
Demented	94.64	94.37	91.78	93.06	88.71
Converted	95.98	84.38	72.97	78.26	76.30
Average	95.00	90.40	87.20	88.64	84.61
Epoch—2500					
Nondemented	94.91	92.54	97.89	95.14	89.95
Demented	94.37	94.96	90.41	92.63	88.15
Converted	96.78	87.88	78.38	82.86	81.25
Average	95.35	91.79	88.89	90.21	86.45
Epoch—3000					
Nondemented	95.71	93.50	98.42	95.90	91.54
Demented	94.64	94.37	91.78	93.06	88.71
Converted	96.78	90.32	75.68	82.35	80.98
Average	95.71	92.73	88.63	90.44	87.08

Table 2. Classifier result of LXAIOA-ADPCM method below various epochs.

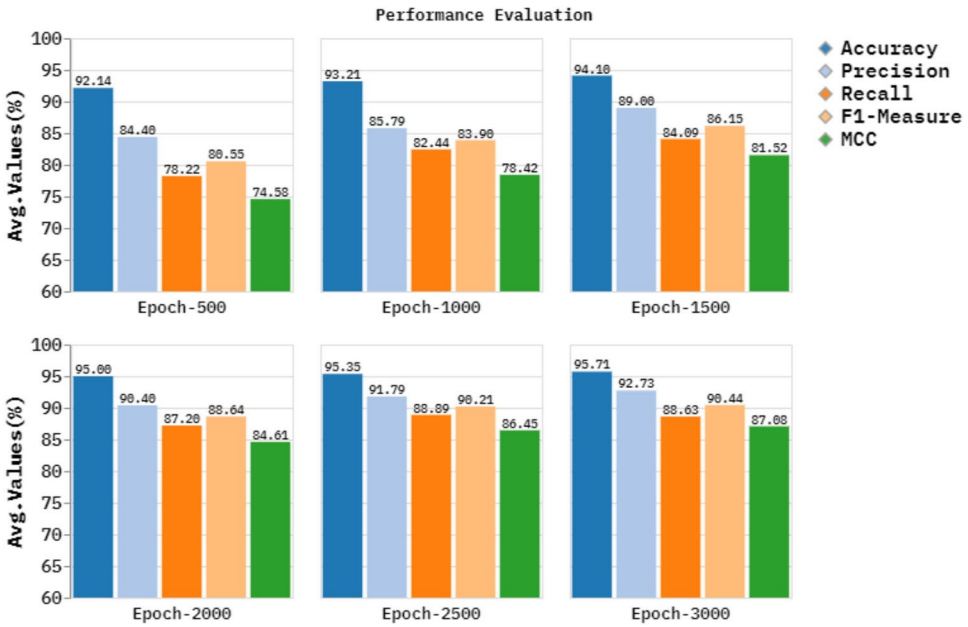

Fig. 4. Average of LXAIOA-ADPCM method under various epochs.

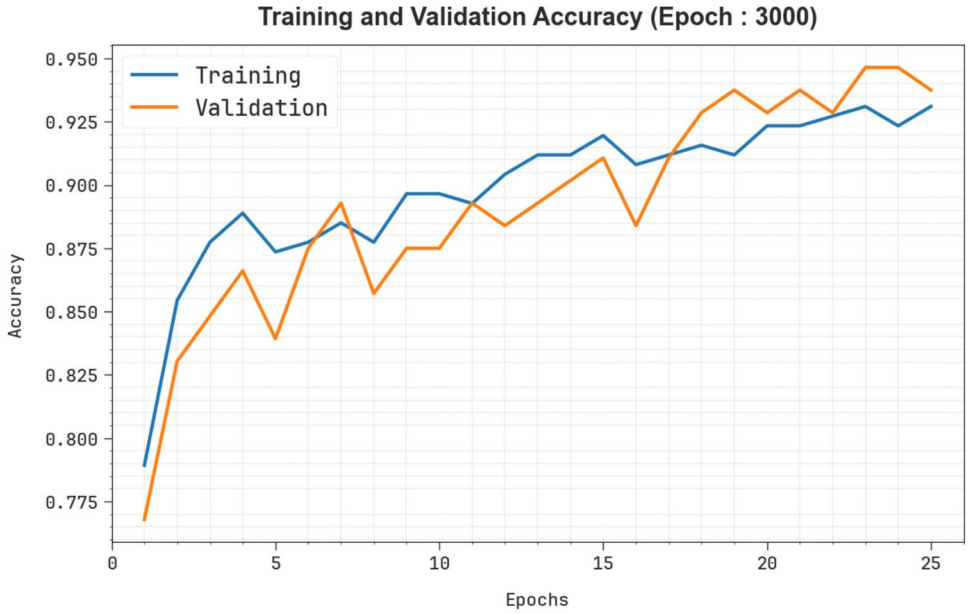

Fig. 5. $Accu_y$ curve of LXAIOA-ADPCM method under epoch 3000.

Fig. 6. Loss analysis of LXAIOA-ADPCM method below epoch 3000.

$F1_{Measure}$ of 88.64%, and MCC of 84.61%. In addition, on epoch 2500, the LXAIOA-ADPCM method reaches an average $accu_y$ of 95.35%, $prec_n$ of 91.79%, $reca_l$ of 88.89%, $F1_{Measure}$ of 90.21%, and MCC of 86.45%. Furthermore, on epoch 3000, the LXAIOA-ADPCM method reaches an average $accu_y$ of 95.71%, $prec_n$ of 92.73%, $reca_l$ of 88.63%, $F1_{Measure}$ of 90.44%, and MCC of 87.08%.

Figure 5 illustrates the training (TRA) $accu_y$ and validation (VAL) $accu_y$ analysis of the LXAIOA-ADPCM method below epoch 3000. The $accu_y$ analysis is calculated across the range of 0–3000 epochs. The outcome highlights that the TRA and VAL $accu_y$ analysis exhibitions an increasing tendency that notifies the capacity of the LXAIOA-ADPCM methodology with superior outcomes across multiple iterations. Simultaneously, the TRA and VAL $accu_y$ leftovers closer across the epochs, which indicates inferior overfitting and exhibitions maximal performance of the LXAIOA-ADPCM methodology, assuring reliable prediction on unseen samples.

Figure 6 shows the TRA loss (TRALOS) and VAL loss (VALLOS) curves of the LXAIOA-ADPCM approach below epoch 3000. The loss values are computed throughout 0–3000 epochs. The TRALOS and VALLOS analysis exemplify a diminishing trend, notifying the capacity of the LXAIOA-ADPCM approach to balance a trade-off

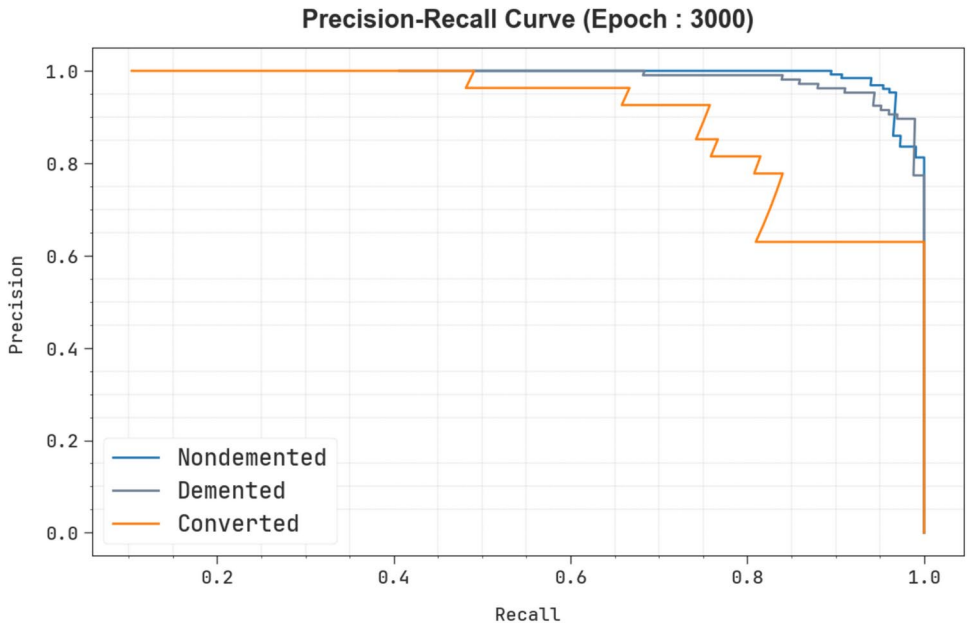

Fig. 7. PR curve of LXAIOA-ADPCM technique under epoch 3000.

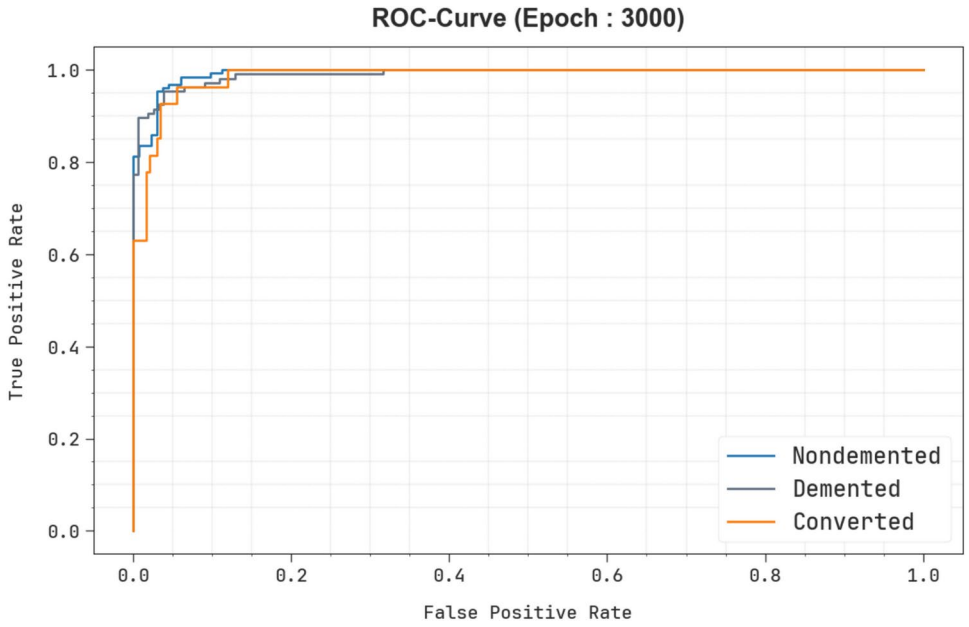

Fig. 8. ROC curve of LXAIOA-ADPCM technique under epoch 3000.

between data fitting and simplification. The continuous reduction in loss values is essential to ensure the more significant outcomes of the LXAIOA-ADPCM model and tune the prediction outcome over time.

In Fig. 7, the PR graph outcomes of the LXAIOA-ADPCM approach below epoch 3000 provide an understanding of its outcomes by plotting Precision beside Recall for each class. The figure demonstrates that the LXAIOA-ADPCM approach continually accomplishes maximum PR analysis over dissimilar class labels, showing its capacity to maintain an essential section of true positive predictions among all positive predictions (precision) while likewise seizing a significant proportion of actual positives (recall).

Figure 8 investigates the ROC graph of the LXAIOA-ADPCM method under epoch 3000. The results imply that the LXAIOA-ADPCM method accomplishes better ROC analysis across every class, demonstrating an essential capacity for discerning classes. This dependable tendency of better ROC analysis across multiple classes suggests the capable performance of the LXAIOA-ADPCM model in predicting classes. The robust nature of the classification procedure is highlighted below.

Classifier	$Accu_{racy}$	$Prec_n$	$Reca_l$	$F1_{Measure}$
RF	91.65	85.01	84.70	89.47
SVC	91.19	89.59	80.09	86.64
AdaBoost	73.03	91.40	82.32	89.41
XGBoost	79.77	85.86	84.07	89.72
MLP Method	91.37	86.90	80.18	87.74
TL-GWO	94.00	85.70	81.06	87.48
ResNet-18	86.96	89.68	83.88	88.59
VGG-16	87.82	89.07	81.40	85.35
Densenet	92.15	85.84	85.33	90.01
PRCNN	91.92	90.19	80.76	87.23
AWD-LSTM	73.63	92.09	83.07	89.21
LXAIOA-ADPCM	95.71	92.73	88.63	90.44

Table 3. Comparative results of LXAIOA-ADPCM methodology with existing methods[27,37–39].

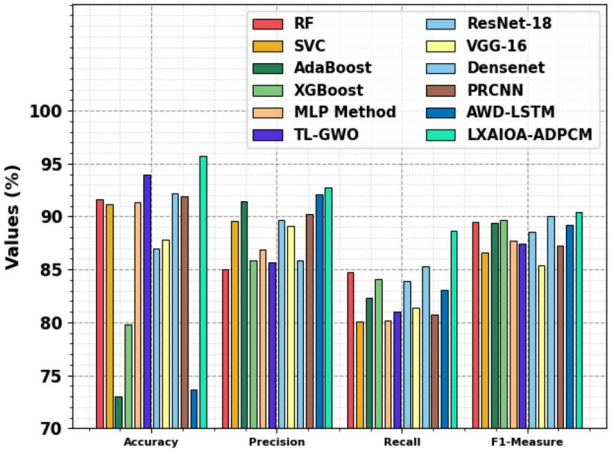

Fig. 9. Comparative outcome of LXAIOA-ADPCM methodology with existing methods.

The comparative results of the LXAIOA-ADPCM technique with existing methodologies are exemplified in Table 3 and Fig. 9[27,37–39]. The simulation outcome stated that the LXAIOA-ADPCM technique outperformed optimal performances. Based on $accu_y$, the LXAIOA-ADPCM technique has a higher $accu_y$ of 95.71%. In contrast, the RF, Support Vector Classification (SVC), AdaBoost, XGBoost, MLP, Transfer Learning (TL)-GWO, ResNet-18, VGG-16, Densenet, PRCNN, and AWD-LSTM methods reached lesser $accu_y$ of 91.65%, 91.19%, 73.03%, 79.77%, 91.37%, 94.00%, 86.96%, 87.82%, 92.15%, 91.92%, and 73.63%, respectively. Moreover, depending on $prec_n$, the LXAIOA-ADPCM technique has greater $prec_n$ of 92.73% whereas the RF, SVC, AdaBoost, XGBoost, MLP, TL-GWO, ResNet-18, VGG-16, Densenet, PRCNN, and AWD-LSTM methods attained minimum $prec_n$ of 85.01%, 89.59%, 91.40%, 85.86%, 86.90%, 85.70%, 89.68%, 89.07%, 85.84%, 90.19%, and 92.09%, correspondingly. Furthermore, based on $reca_l$, the LXAIOA-ADPCM approach attained higher $reca_l$ of 88.63%, whereas the RF, SVC, AdaBoost, XGBoost, MLP, TL-GWO, ResNet-18, VGG-16, Densenet, PRCNN, and AWD-LSTM methods reached lesser $reca_l$ of 84.70%, 80.09%, 82.32%, 84.07%, 80.18%, 81.06%, 83.88%, 81.40%, 85.33%, 80.76%, and 83.07%, subsequently. Also, depending on $F1_{Measure}$, the LXAIOA-ADPCM approach has a superior $F1_{Measure}$ of 90.44%, whereas the RF, SVC, AdaBoost, XGBoost, MLP, TL-GWO, ResNet-18, VGG-16, Densenet, PRCNN, and AWD-LSTM methods attained worst $F1_{Measure}$ of 89.47%, 86.64%, 89.41%, 89.72%, 87.74%, 87.48%, 88.59%, 85.35%, 90.01%, 87.23%, and 89.21%, correspondingly.

Table 4 and Fig. 10 illustrate the time-consuming (TC) of the LXAIOA-ADPCM method with existing classifiers. The proposed LXAIOA-ADPCM method gets a minimal TC value of 4.40 s. Meanwhile, the existing methodologies, such as RF, SVC, AdaBoost, XGBoost, MLP, TL-GWO, ResNet-18, VGG-16, Densenet, PRCNN, and AWD-LSTM techniques, attain greater TC values of 11.13 s, 8.04 s, 11.52 s, 15.90 s, 13.52 s, 13.69 s, 12.13 s, 8.12 s, 10.34 s, 7.65 s, and 9.01 s, respectively.

Conclusion

In this paper, an LXAIOA-ADPCM methodology for medical diagnosis is proposed. The main intention of the LXAIOA-ADPCM methodology is to progress a novel technique for dementia prediction using advanced

Classifier	TC (s)
RF	11.13
SVC	8.04
AdaBoost	11.52
XGBoost	15.90
MLP Method	13.52
TL-GWO	13.69
ResNet-18	12.13
VGG-16	8.12
Densenet	10.34
PRCNN	7.65
AWD-LSTM	9.01
LXAIOA-ADPCM	4.40

Table 4. TC outcome of LXAIOA-ADPCM approach with existing models.

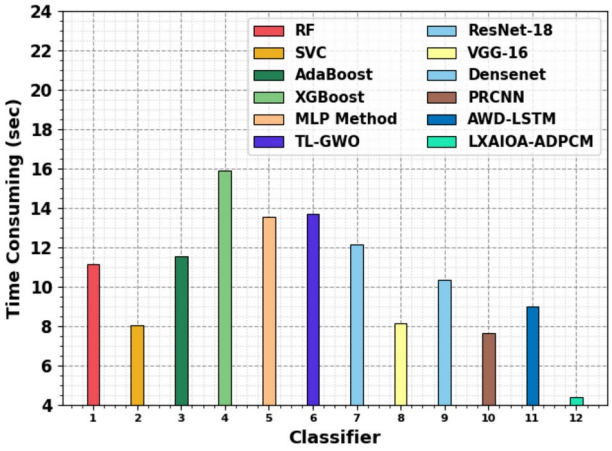

Fig. 10. TC outcome of LXAIOA-ADPCM approach with existing models.

techniques. Initially, the data normalization stage employs min–max normalization for converting input data into a beneficial format. Moreover, the FS process is performed by implementing the NMRA technique. The proposed LXAIOA-ADPCM model implements ensemble classifiers such as the BiLSTM, SAE, and TCN techniques for the classification process. Furthermore, the hyperparameter selection of ensemble models is performed by utilizing the GOA model. Finally, Grad-CAM is employed as an XAI technique to enhance transparency by providing human-understandable insights into their decision-making processes. A broad array of experiments using the LXAIOA-ADPCM technique is performed under the Dementia Prediction dataset. The simulation validation of the LXAIOA-ADPCM technique portrayed a superior accuracy output of 95.71% over existing models. The limitations of the LXAIOA-ADPCM technique comprise the reliance on a single dataset, which may restrict the generalizability of the findings across diverse populations. Additionally, while the method exhibits high accuracy, its computational complexity may pose challenges in real-time applications. The interpretability of some models remains a concern, specifically in clinical settings where transparency is crucial. Furthermore, the model's capability to handle noisy or incomplete data has not been extensively tested. Future work could concentrate on expanding the dataset to comprise more diverse samples, optimizing computational efficiency, and improving the explainability of the models for broader clinical adoption. Further validation in clinical trials is also required to confirm its robustness in practical healthcare environments.

Data availability

The data supporting this study's findings are openly available in the Kaggle repository at https://www.kaggle.com/datasets/shashwatwork/dementia-prediction-dataset, reference number[36].

Received: 17 February 2025; Accepted: 2 April 2025
Published online: 13 May 2025

References

1. Javeed, A. et al. Machine learning for dementia prediction: A systematic review and future research directions. *J. Med. Syst.* **47**(1), 17 (2023).

2. James, C., Ranson, J. M., Everson, R. & Llewellyn, D. J. Performance of machine learning algorithms for predicting progression to dementia in memory clinic patients. *JAMA Netw. Open* **4**(12), e2136553–e2136553 (2021).
3. Spooner, A. et al. A comparison of machine learning methods for survival analysis of high-dimensional clinical data for dementia prediction. *Sci. Rep.* **10**(1), 20410 (2020).
4. Lanskey, J. H. et al. Can neuroimaging predict dementia in Parkinson's disease?. *Brain* **141**(9), 2545–2560 (2018).
5. Battineni, G., Chintalapudi, N. & Amenta, F. Machine learning in medicine: Performance calculation of dementia prediction by support vector machines (SVM). *Inf. Med. Unlocked* **16**, 100200 (2019).
6. Hou, X. H. et al. Models for predicting risk of dementia: A systematic review. *J. Neurol. Neurosurg. Psychiatry* **90**(4), 373–379 (2019).
7. Pemberton, H. G. et al. Technical and clinical validation of commercial automated volumetric MRI tools for dementia diagnosis—A systematic review. *Neuroradiology* **63**(11), 1773–1789 (2021).
8. Aschwanden, D. et al. Predicting cognitive impairment and dementia: A machine learning approach. *J. Alzheimers Dis.* **75**(3), 717–728 (2020).
9. Gill, S. et al. Using machine learning to predict dementia from neuropsychiatric symptom and neuroimaging data. *J. Alzheimers Dis.* **75**(1), 277–288 (2020).
10. Sameh, B., Khodadadi, N., Eid, M. M. & Towfek, S. K. Advancements and future directions in machine learning for medical diagnostics: A comprehensive review. *Full Length Article* **7**(2), 18–28 (2024).
11. Kang, W., Jiskoot, L., De Deyn, P., Biessels, G., Koek, H., Claassen, J., Middelkoop, H., Flier, W., Jansen, W.J., Klein, S. and Bron, E., 2025. GL-ICNN: An End-To-End Interpretable Convolutional Neural Network for the Diagnosis and Prediction of Alzheimer's Disease. Preprint at arXiv preprint arXiv:2501.11715.
12. Saleh, H., ElRashidy, N., Abd Elaziz, M., Aseeri, A. O. & El-Sappagh, S. Genetic algorithm-based hybrid deep learning model for explainable Alzheimer's disease prediction using temporal multimodal cognitive data. *Int. J. Data Sci. Anal.* https://doi.org/10.1007/s41060-024-00514-z (2024).
13. Arshad Choudhry, I. et al. A novel interpretable graph convolutional neural network for multimodal brain tumor segmentation. *Cogn. Comput.* **17**(1), 1–25 (2025).
14. AbdelAziz, N. M., Said, W., AbdelHafeez, M. M. & Ali, A. H. Advanced interpretable diagnosis of Alzheimer's disease using SECNN-RF framework with explainable AI. *Front. Artif. Intell.* **7**, 1456069 (2024).
15. Bazine, O. et al. Convolutional cross-modal autoencoder-based few-shot learning for data augmentation with application to Alzheimer dementia diagnosis. *Cogn. Comput.* **17**(1), 34 (2025).
16. Kamal, M. S., & Nimmy, S. F. Interpretable transformers for Alzheimer disease diagnosis on multimodal data. In *2024 International Joint Conference on Neural Networks (IJCNN)* (pp. 1–8). IEEE (2024).
17. Khanom, F., Uddin, M. S. & Mostafiz, R. PD_EBM: An integrated boosting approach based on selective features for unveiling parkinson's disease diagnosis with global and local explanations. *Eng. Rep.* **7**(1), e13091 (2025).
18. Adarsh, V., Gangadharan, G. R., Fiore, U. & Zanetti, P. Multimodal classification of Alzheimer's disease and mild cognitive impairment using custom MKSCDDL kernel over CNN with transparent decision-making for explainable diagnosis. *Sci. Rep.* **14**(1), 1774 (2024).
19. Alhussen, A. et al. Early attention-deficit/hyperactivity disorder (ADHD) with NeuroDCT-ICA and rhinofish optimization (RFO) algorithm based optimized ADHD-AttentionNet. *Sci. Rep.* **15**(1), 6967 (2025).
20. Zhang, C. et al. Hematoma evacuation via image-guided para-corticospinal tract approach in patients with spontaneous intracerebral hemorrhage. *Neurol. Ther.* **10**, 1001–1013 (2021).
21. Pei, J. et al. Quercetin-functionalized nanomaterials: Innovative therapeutic avenues for Alzheimer's disease management. *Ageing Res. Rev.* **104**, 102665 (2025).
22. Pan, H., Li, Z., Fu, Y., Qin, X. & Hu, J. Reconstructing visual stimulus representation from EEG signals based on deep visual representation model. *IEEE Trans. Hum. Mach. Syst.* **54**, 711 (2024).
23. Pan, H., Tong, S., Song, H. & Chu, X. A miner mental state evaluation scheme with decision level fusion based on multidomain EEG information. *IEEE Trans. Hum. Mach. Syst.* **55**, 289 (2025).
24. Wang, L. et al. Neuroendoscopic parafascicular evacuation of spontaneous intracerebral hemorrhage (NESICH technique): A multicenter technical experience with preliminary findings. *Neurol. Ther.* **13**(4), 1259–1271 (2024).
25. Li, L. et al. Nanozyme-enhanced tyramine signal amplification probe for preamplification-free myocarditis-related miRNAs detection. *Chem. Eng. J.* **503**, 158093 (2025).
26. Chauhan, P. et al. PBVit: A patch-based vision transformer for enhanced brain tumor detection. *IEEE Access* **13**, 13015 (2024).
27. Walha, A. et al. Deep learning and machine learning architectures for dementia detection from speech in women. *Comput. Model. Eng. Sci.* **142**(3), 2959 (2025).
28. Freja, S. A., & Hallaj, Y. *Early Dementia Detection in Speech Transcripts Using Machine Learning and Large Language Models* (Master's thesis, UIS). (2024)
29. Shantal, M., Othman, Z. & Bakar, A. A. A novel approach for data feature weighting using correlation coefficients and min-max normalization. *Symmetry* **15**(12), 2185 (2023).
30. Sharma, P., Salgotra, R., Raju, S., Abouhawwash, M. & Askar, S. S. A hybrid Prairie INFO fission naked algorithm with stagnation mechanism for the parametric estimation of solar photovoltaic systems. *Sci. Rep.* **15**(1), 4001 (2025).
31. Chu, T. S., & Ashraf, M. Detecting intrusion in Internet of Things (Iot) with deep learning bi-directional recurrent neural network (BRNN)
32. Cywiński, B., & Deja, K. SAeUron: Interpretable concept unlearning in diffusion models with sparse autoencoders. Preprint at arXiv:2501.18052. (2025)
33. Zare, M. S., Nikoo, M. R., Chen, M. & Gandomi, A. H. Capturing complex electricity load patterns: A hybrid deep learning approach with proposed external-convolution attention. *Energ. Strat. Rev.* **57**, 101638 (2025).
34. Biswas, S. et al. Integrating Differential Evolution into Gazelle Optimization for advanced global optimization and engineering applications. *Comput. Methods Appl. Mech. Eng.* **434**, 117588 (2025).
35. Biswas, S., Mostafiz, R., Uddin, M. S. & Paul, B. K. XAI-FusionNet: Diabetic foot ulcer detection based on multi-scale feature fusion with explainable artificial intelligence. *Heliyon* **10**(10), e31228 (2024).
36. https://www.kaggle.com/datasets/shashwatwork/dementia-prediction-dataset
37. Kuo, P. H., Huang, C. T. & Yao, T. C. Optimized transfer learning based dementia prediction system for rehabilitation therapy planning. *IEEE Trans. Neural Syst. Rehabil. Eng.* **31**, 2047–2059 (2023).
38. Jain, V. et al. A novel AI-based system for detection and severity prediction of dementia using MRI. *IEEE Access* **9**, 154324–154346 (2021).
39. Ryu, S. E., Shin, D. H. & Chung, K. Prediction model of dementia risk based on XGBoost using derived variable extraction and hyper parameter optimization. *IEEE Access* **8**, 177708–177720 (2020).

Acknowledgements

The authors extend their appreciation to the Deanship of Research and Graduate Studies at King Khalid University for funding this work through Large Research Project under grant number RGP2/461/45. Princess Nourah bint Abdulrahman University Researchers Supporting Project number (PNURSP2025R809), Princess Nourah

bint Abdulrahman University, Riyadh, Saudi Arabia. The authors extend their appreciation to the Deanship of Scientific Research at Northern Border University, Arar, KSA for funding this research work through the project number "NBU-FFR-2025-2932-02. The authors are thankful to the Deanship of Graduate Studies and Scientific Research at University of Bisha for supporting this work through the Fast-Track Research Support Program. This study is supported via funding from Prince Sattam bin Abdulaziz University project number (PSAU/2025/R/1446).

Author contributions

Conceptualization: Mohamed Medani Data curation and Formal analysis: Ghada Moh. Samir Elhessewi, Mohammed Assiri Investigation and Methodology: Mohamed Medani, Mohammed Alqahtani Funding Support, Somia A. Asklany, Menwa Alshammeri Project administration and Resources: Supervision; Somia A. Asklany Validation and Visualization: Sulaiman Alamro, Da'ad Albalawneh Writing—original draft, Mohamed Medani Writing—review and editing, Somia A. Asklany, Menwa Alshammeri All authors have read and agreed to the published version of the manuscript.

Declarations

Competing interests

The authors declare no competing interests.

Additional information

Correspondence and requests for materials should be addressed to S.A.A.

Reprints and permissions information is available at www.nature.com/reprints.

Publisher's note Springer Nature remains neutral with regard to jurisdictional claims in published maps and institutional affiliations.